State-dependent Inactivation of the α1G T-Type Calcium Channel

Jose R. Serrano,* Edward Perez-Reyes,‡ and Stephen W. Jones*

From the *Department of Physiology and Biophysics, Case Western Reserve University, Cleveland, Ohio 44106; and the ‡Department of Physiology, Loyola University Medical Center, Maywood, Illinois 60153

abstract We have examined the kinetics of whole-cell T-current in HEK 293 cells stably expressing the α1G channel, with symmetrical Na^+_i and Na^+_o and 2 mM Ca^{2+}_o. After brief strong depolarization to activate the channels (2 ms at +60 mV; holding potential −100 mV), currents relaxed exponentially at all voltages. The time constant of the relaxation was exponentially voltage dependent from −120 to −70 mV (e-fold for 31 mV; τ = 2.5 ms at −100 mV), but τ = 12–17 ms from −40 to +60 mV. This suggests a mixture of voltage-dependent deactivation (dominating at very negative voltages) and nearly voltage-independent inactivation. Inactivation measured by test pulses following that protocol was consistent with open-state inactivation. During depolarizations lasting 100–300 ms, inactivation was strong but incomplete (∼98%). Inactivation was also produced by long, weak depolarizations (τ = 220 ms at −80 mV; $V_{1/2}$ = −82 mV), which could not be explained by voltage-independent inactivation exclusively from the open state. Recovery from inactivation was exponential and fast (τ = 85 ms at −100 mV), but weakly voltage dependent. Recovery was similar after 60-ms steps to −20 mV or 600-ms steps to −70 mV, suggesting rapid equilibration of open- and closed-state inactivation. There was little current at −100 mV during recovery from inactivation, consistent with ≤8% of the channels recovering through the open state. The results are well described by a kinetic model where inactivation is allosterically coupled to the movement of the first three voltage sensors to activate. One consequence of state-dependent inactivation is that α1G channels continue to inactivate after repolarization, primarily from the open state, which leads to cumulative inactivation during repetitive pulses.

key words: T-channel • cumulative inactivation • recovery from inactivation

introduction

Voltage-dependent Ca^{2+} channels provide a pathway for rapid influx of Ca^{2+} into cells, which plays a crucial role in both electrical and metabolic signaling. Electrophysiological studies have identified two primary channel types, high voltage-activated (HVA)[1] and low voltage-activated (LVA, or T-type) channels (Bean, 1989). Beginning in 1987, the cloning of several HVA channels allowed detailed study of their properties (Catterall, 1996), but the molecular basis of T-channels proved more elusive. The recent cloning of α1G, which exhibits the key functional properties of T-channels when expressed in *Xenopus* oocytes (Perez-Reyes et al., 1998), was an important step toward understanding the biology of T-channels.

T-Channels have been distinguished from HVA channels by a set of biophysical properties, including a more negative voltage range for both activation and inactivation, rapid and nearly complete inactivation, and relatively slow channel closing upon repolarization (deactivation) (Carbone and Lux, 1984; Armstrong and Matteson, 1985; Fox et al., 1987). T-channels also have a lower single channel conductance in isotonic Ba^{2+}, and differ from most HVA channels in selectivity among divalent cations for permeation and block (Bean, 1985; Nilius et al., 1985; Nowycky et al., 1985; Narahashi et al., 1987). The kinetic properties of T-channels suggest a key role in regulating electrical activity in the critical voltage region near threshold. For example, T-channels are involved in generation of bursts of action potentials in thalamic neurons (Huguenard, 1996).

Significant heterogeneity has been observed in the kinetics of T-channel gating, particularly inactivation rates and the voltage dependence of steady state inactivation (Huguenard, 1996). This may be partially explained by use of different experimental conditions, notably the nonphysiological ionic conditions often required to isolate T-current from currents through other ion channels. However, T-currents can genuinely differ in kinetics and pharmacology among cell types (Chen and Hess, 1990; Huguenard and Prince, 1992; Todorovic and Lingle, 1998). This may reflect the emerging molecular diversity among T-channels, with three clones (α1G, α1H, and α1I) known to date (Perez-Reyes et al., 1998; Cribbs et al., 1998; Lee et al., 1999).

Cloned T-channels have putative S4 transmembrane regions, suggesting that the mechanism of voltage-

Address correspondence to Stephen W. Jones, Department of Physiology and Biophysics, Case Western Reserve University, Cleveland, OH 44106. Fax: 216-368-3952; E-mail: swj@po.cwru.edu

[1]*Abbreviations used in this paper:* HVA, high voltage-activated; LVA, low voltage-activated; k_I, rate constant for inactivation from the open state; k_{-I}, rate constant for recovery from inactivation (to the open state); k_C, rate constant for channel closing; P_O, probability that a channel is open; $P_{O,r}$, P_O relative to that produced by a 2-ms depolarization from −100 to +60 mV; P_I, probability that a channel is inactivated.

dependent activation is essentially the same as in other members of the extended family of K^+, Na^+, and Ca^{2+} channels. However, little is known about the mechanism of inactivation in T-channels, or its relationship to the various fast and slow voltage-dependent inactivation processes known for other channels. T-channel inactivation has been described either by models based on Hodgkin and Huxley (1952b) that assume intrinsically voltage-dependent inactivation (Wang et al., 1991; Huguenard and McCormick, 1992), or by state-dependent inactivation (Chen and Hess, 1990).

The goal of this study was to characterize the gating of T-channels using whole-cell recording from HEK 293 cells stably expressing the α1G clone, with emphasis on the kinetics of inactivation. In this system, it was possible to characterize T-currents over a wide voltage range, under nearly normal ionic conditions (notably, 2 mM Ca^{2+} as the charge carrier). We found that α1G channels inactivate primarily from the open state, although inactivation at hyperpolarized voltages involves "partially activated" closed states, and the main pathway for recovery from inactivation bypasses the open state. The currents show strong cumulative inactivation in response to repetitive depolarizations, consistent with continued inactivation from the open state even after repolarization.

materials and methods

Cell Culture

Generation of the stable HEK 293 cell line expressing rat α1G (sequence data available from EMBL/GenBank/DDBJ under accession no. AF027984) has been described previously (Lee et al., 1999). Cells were cultured in MEM supplemented with 10% fetal bovine serum and 600 μg/ml G418, at 37°C in 95% O_2, 5% CO_2. Cell culture media and reagents were from GIBCO BRL. The cells were passaged every 3–4 d. Before recording, cells were harvested from the culture dish by trypsinization, washed with MEM, and stored in the supplemented medium. Cells were used for patch clamp recording 1–4 d after trypsinization.

Electrophysiology

Currents were recorded using conventional whole-cell patch clamp recording, with an Axopatch 200A amplifier and the Clampex program of pClamp v. 6.0.3 (Axon Instruments). The extracellular solution was 140 mM NaCl, 2 mM $CaCl_2$, 1 mM $MgCl_2$, and 10 mM HEPES, adjusted to pH 7.2 with NaOH. The intracellular solution contained 140 mM NaCl, 11 mM EGTA, 2 mM $CaCl_2$, 4 mM MgATP, 1 mM $MgCl_2$, and 10 mM HEPES, pH 7.2 with NaOH. The pipets filled with intracellular solution had resistances of 2–4 MΩ. The series resistance in the whole-cell configuration (measured from optimal compensation of capacity transients with the amplifier circuitry) was 5.7 ± 0.3 MΩ, with cell capacitance of 15.3 ± 0.5 pF (n = 26). Series resistance compensation was nominally 80–90%. All experiments were performed at room temperature (~20°C).

The holding potential was −100 mV. Currents were recorded on two channels, with on-line leak subtraction using the $P/-4$ method on one channel, and raw data during depolarizations on the other, to assess the holding current and cell stability. When this is done, Clampex v. 6 incorrectly sets the current to zero at the end of each leak-subtracted record, so all protocols included a significant period of time at the holding potential at the beginning of each record, and the current during that first holding level was set to zero when the leak-subtracted data were analyzed (using Analyze Adjust Baseline for Epoch A in Clampfit).

Data Analysis

Most data analysis used Clampfit v. 6. Exponential fits to data records used the Simplex or Mixed methods of Clampfit. Other curve fitting was done with the Solver function of Microsoft Excel v. 5 or Excel 97. Unless noted otherwise, values are mean ± SEM. For figures showing averaged data, error bars (±SEM) are shown when larger than the symbols.

Since the currents recorded could be >1 nA, data were examined closely for signs of series resistance error. Clamp speed was assessed by the rise time of tail currents, and steady state accuracy by the effect of partial inactivation on the time course of tail currents. For cells used for kinetic analysis of tail currents (e.g., Fig. 3), the 10–90% rise time was 0.15–0.35 ms after 10-kHz analogue filtering. Prepulses that caused ~70% inactivation (using the protocol illustrated in the inset to Fig. 11) affected the time constant for deactivation at −100 mV by ≤15%. Since the measured time constants changed 37% per 10 mV near −100 mV (see Fig. 5), this suggests ≤5 mV error.

Kinetic models were simulated using SCoP (v. 3.51; Simulation Resources). Simulated data were analyzed further using spreadsheets, or were converted to binary files and analyzed with Clampfit.

results

General Characteristics of Macroscopic Currents

Currents with the properties expected of T-type calcium currents were recorded from HEK 293 cells stably expressing α1G cDNA. Depolarizations in 10-mV increments from a holding potential of −100 mV elicited transient inward and outward currents (Fig. 1 A). Currents showed voltage-dependent macroscopic activation and inactivation, with faster kinetics at more depolarized voltages. At intermediate voltages, the currents "cross over" as typically observed for Na^+ currents and T-currents (Randall and Tsien, 1997; Perez-Reyes et al., 1998). The current–voltage (I–V) relationship, measured at the time of peak current during each record, is shown in Fig. 1 B. Detectable current was first observed near −70 mV, with peak inward current near −40 mV.

The ionic conditions used in this study were essentially normal (see materials and methods), including 2 mM Ca^{2+}_o, except that K^+_i was replaced by Na^+_i to minimize currents through any endogenous K^+ channels that might be present. HEK 293 cells have occasionally been reported to have endogenous ion channels (Berjukow et al., 1996; Zhu et al., 1998), which could interfere with study of heterologously expressed channels. Especially since the outward currents at positive voltages were unexpectedly large (Fig. 1), we evaluated the presence of contaminating currents using the "envelope" of

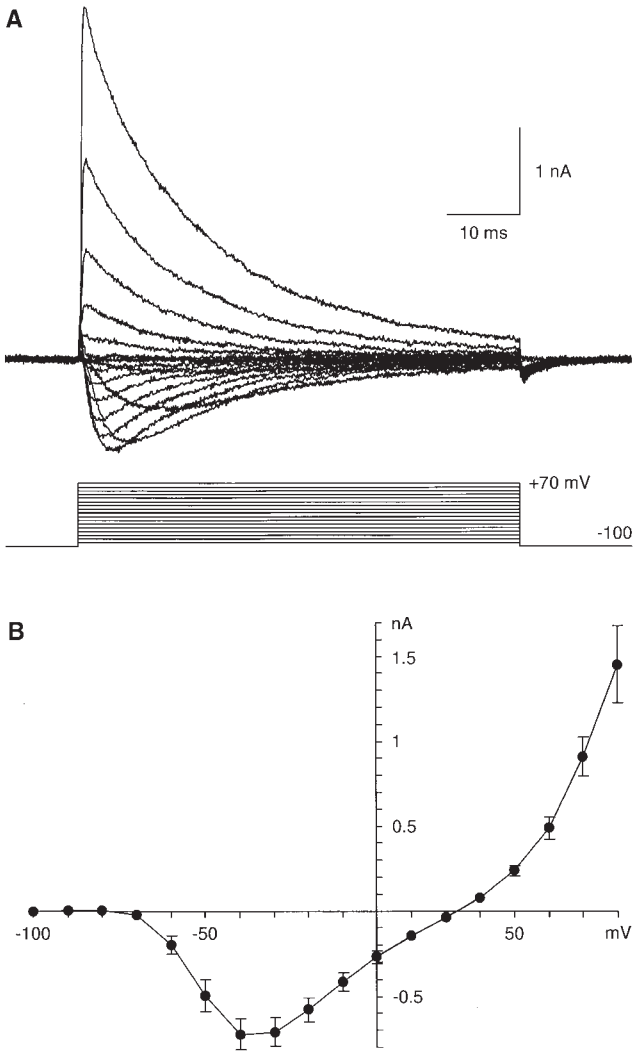

Figure 1. Current–voltage relations for α1G channels. (A) Sample current records, with 5 kHz Gaussian filtering, from cell e8612. (B) Current–voltage relations averaged from 12 cells, measured at the point of peak current at each voltage.

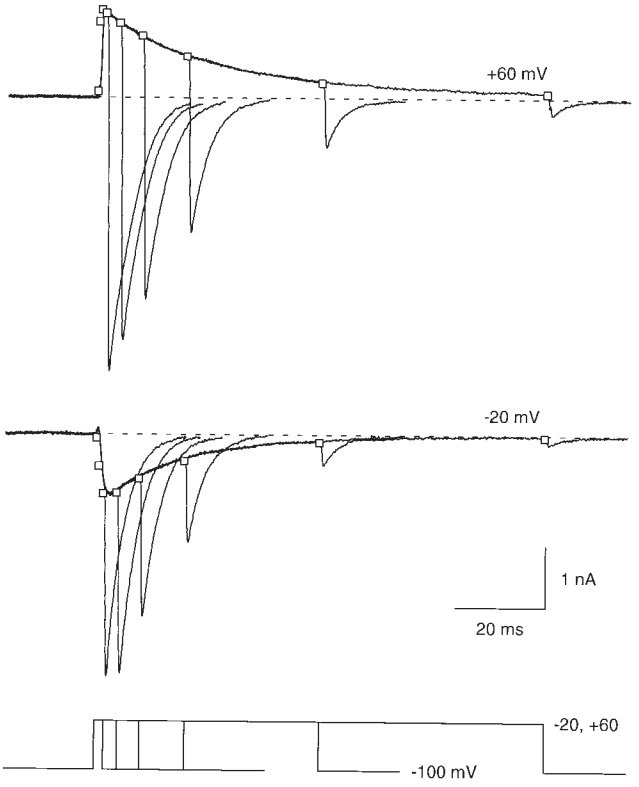

Figure 2. Envelope test for isolation of α1G currents. Depolarizations of variable duration were given to +60 mV (above) or −20 mV (below). The records shown lasted 2, 5, 10, 20, 50, and 100 ms. The peak amplitudes of the tail currents after repolarization for those records (and for steps lasting 0.2, 0.5, and 1 ms) were scaled to match the currents during depolarization, and are shown as open squares superimposed on the records. Cell a8612, 3 kHz Gaussian filtering.

tail currents produced by depolarizations of different durations. If the recorded currents reflect activity of a single class of channel, the peak amplitude of a tail current must be proportional to the amplitude of the current at the end of the preceding voltage step (Hodgkin and Huxley, 1952a). Fig. 2 demonstrates that the tail currents change in parallel with the step current, and that the tail current amplitudes multiplied by a constant scaling factor superimpose on the time course of the current recorded during the step, for steps to −20 or +60 mV. These data indicate that the α1G currents are well isolated in our experimental conditions.

The I–V curve, measured as in Fig. 1 B, is affected both by gating (activation and inactivation) and by permeation (the voltage dependence of ion flow through an open channel). The protocol of Fig. 3 A was used to begin to separate those processes. Channels were first activated by a 2-ms pulse to +60 mV, designed to rapidly activate the channels while minimizing inactivation. This protocol allows us to examine permeation, from the instantaneous I–V relation measured immediately after repolarization (Fig. 3 B). Assuming that the brief step to +60 mV activates the same number of channels each time (consistent with the constancy of the current recorded during the step to +60 mV), the shape of the instantaneous I–V should reflect the voltage dependence of current flow through an open channel. This I–V is distinctly nonlinear, suggesting complex interactions among permeant ions in the α1G pore. The reversal potential was +24.4 ± 1.3 mV (n = 8), similar to previous reports for native T-channels (Fukushima and Hagiwara, 1985; Lux et al., 1990). That relatively low selectivity, corresponding to P_{Ca}/P_{Na} = 105, results in part from the use of Na^+_i, since α1G is approximately threefold selective for Na^+ over Cs^+ (Dashti et al., 1999), as observed for native T-chan-

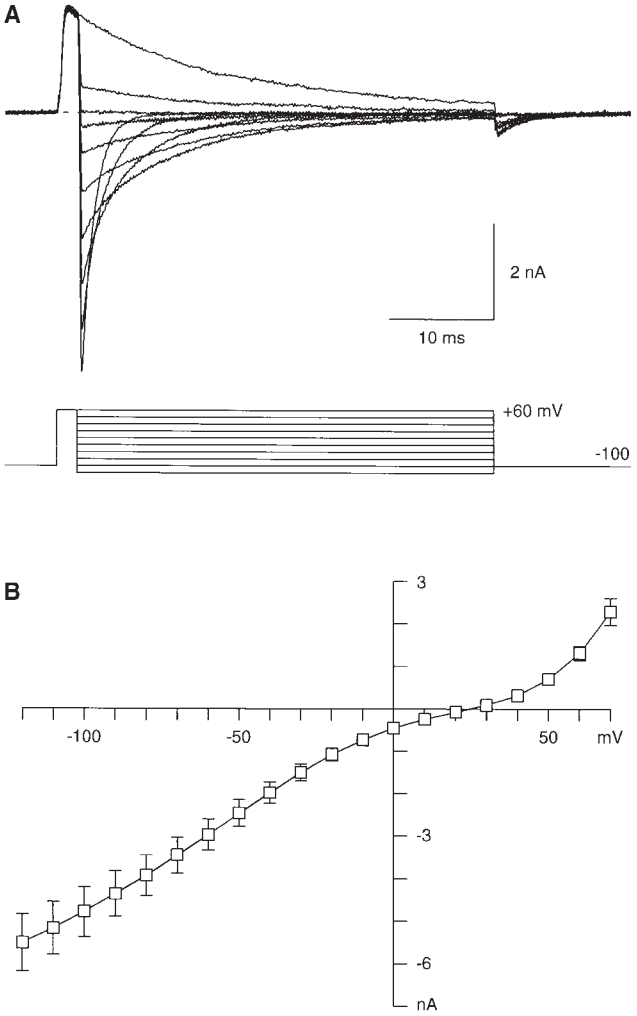

Figure 3. Instantaneous current–voltage relations for α1G channels. (A) Sample current records, with 5 kHz Gaussian filtering, from cell e8612. The initial step to +60 mV lasted 2 ms. Records are shown for repolarizations in 20-mV increments. 2-ms test pulses to +60 mV were given at the end of the protocol, 20-ms after repolarization to −100 mV, to assess inactivation (not shown; see Fig. 11 below). (B) Instantaneous current–voltage relations, measured from the protocol of A, averaged from eight cells. Currents were measured at the peak of the tail current in each cell, which varied from 0.3 to 0.5 ms in these cells.

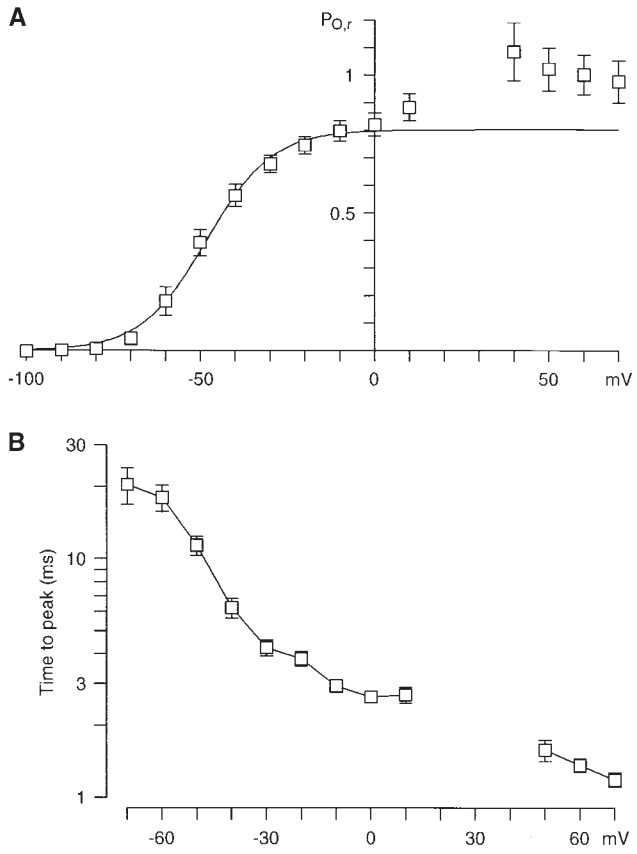

Figure 4. Activation of α1G channels. (A) Activation curve, from current ratios: the peak current recorded during depolarization directly to the indicated voltage (the protocol of Fig. 1), divided by the instantaneous current recorded after repolarization from a 2-ms step to +60 mV (the protocol of Fig. 3). Data are not shown for voltages near the reversal potential. $n = 7$ (except $n = 6$ at +10 mV). The smooth curve is a fit to a Boltzmann functions: $V_{1/2} = -48$ mV, e-fold for 9.4 mV, amplitude 0.80. (B) Time to peak, for the protocol of Fig. 1, $n = 7$.

nels (Fukushima and Hagiwara, 1985; Lux et al., 1990) and L-channels (Hess et al., 1986).

Division of the I–V curve (Fig. 1 B) by the instantaneous I–V curve (Fig. 3 B) was used to evaluate the voltage dependence of activation of α1G channels (Fig. 4 A). That ratio ($P_{O,r}$) should be proportional to the number of channels open at the time of peak current at each voltage. Compared with the usual procedure of measuring tail current amplitudes after depolarizations of fixed duration, this method has the advantage of measuring activation at the maximal value for each voltage. The data at ≤0 mV were fitted to a single Boltzmann function, with half-maximal activation at −48 mV. The data deviate from that function at positive voltages, in part because the current ratios become discontinuous at the reversal potential, but the measured activation was consistently ~20% greater near +60 mV than near 0 mV. For a rapidly inactivating channel, some channels will inactivate before the point of peak inward current, and the extent of that "hidden" inactivation may vary with voltage. Therefore, the activation curve (Fig. 4 A) should be considered an empirical measurement, which may not fully describe the true voltage dependence of the microscopic activation process.

The time course of channel activation was nonexponential. At negative voltages, there was a clear sigmoid delay, which could be approximated by m^2h or m^3h kinetics (not shown). At positive voltages, the initial time course was not well resolved because of a transient outward current, possibly a gating current, which lasted

<1 ms at the T-current reversal potential. The time to peak was voltage dependent, changing approximately fourfold over 100 mV from −30 to +70 mV (Fig. 4 B).

Voltage Dependence of Inactivation and Deactivation

Macroscopic inactivation was measured by single exponential fits to the time course of current decay using the protocol of Fig. 1 (filled symbols, Fig. 5 A). Inactivation was relatively slow at more negative voltages (−60 to −40 mV), but varied little with voltage between −30 and +70 mV. One explanation is that the microscopic inactivation process is voltage independent, as proposed for Na^+ channels (Armstrong and Bezanilla, 1977), but macroscopic inactivation is voltage dependent because of kinetic coupling to the activation process, especially at relatively negative voltages where activation is incomplete. To test that idea, time constants were also measured for the relaxations from the protocol of Fig. 3 (open symbols, Fig. 5 A). The decay of current in that case reflects a combination of channel closing (deactivation) and inactivation. From −120 to −70 mV, where channels would be expected to deactivate, the time constants varied exponentially with voltage (e-fold for 31.1 ± 0.4 mV, $n = 8$; $\tau = 2.5 \pm 0.2$ ms at −100 mV). At more depolarized voltages, the time constants varied little (from $\tau = 11.6 \pm 0.6$ ms at −40 mV to $\tau = 16.6 \pm 1.1$ ms at +60 mV), and were comparable to the time constants for macroscopic inactivation. These results are consistent with voltage-dependent channel closing, dominating at extreme negative voltages, but nearly voltage-independent inactivation. There was actually a slight increase in the time constant for inactivation with depolarization (∼20% from −20 to +60 mV; Fig. 5 A).

The rate of T-channel deactivation reaches a voltage-independent limiting rate at extreme negative voltages in some studies (Chen and Hess, 1990) but not others (Herrington and Lingle, 1992; Todorovic and Lingle, 1998). To test this for α1G, we examined tail currents at voltages as negative as −150 mV. The time constants showed no detectable deviation from exponential voltage dependence (Fig. 5 B).

Inactivation and Recovery at Negative Voltages

Substantial inactivation was observed at voltages as negative as −80 mV (Fig. 6 A). Pulses to −120 mV had little effect, implying that there is little resting fast inactivation at our holding potential of −100 mV. At −80 mV, inactivation proceeded with $\tau = 223 \pm 26$ ms, and was 70 ± 5% complete ($n = 5$). Inactivation was nearly complete at −70 mV (94 ± 5%, with $\tau = 237 \pm 39$ ms, $n = 6$).

We examined the time and voltage dependence of recovery from inactivation (Fig. 6 B), using the protocol illustrated in Fig. 6 C. Recovery from inactivation was complete at −100 and −120 mV. Strikingly, the time course was essentially identical at those voltages (Table I), suggesting voltage-independent recovery from inactivation at voltages where recovery is complete. Recovery was incomplete, but only slightly slower, at −90 and −80 mV (Table I).

Fig. 6 suggests that inactivation should reach a steady state by ∼1 s. To test that, and to measure the proper-

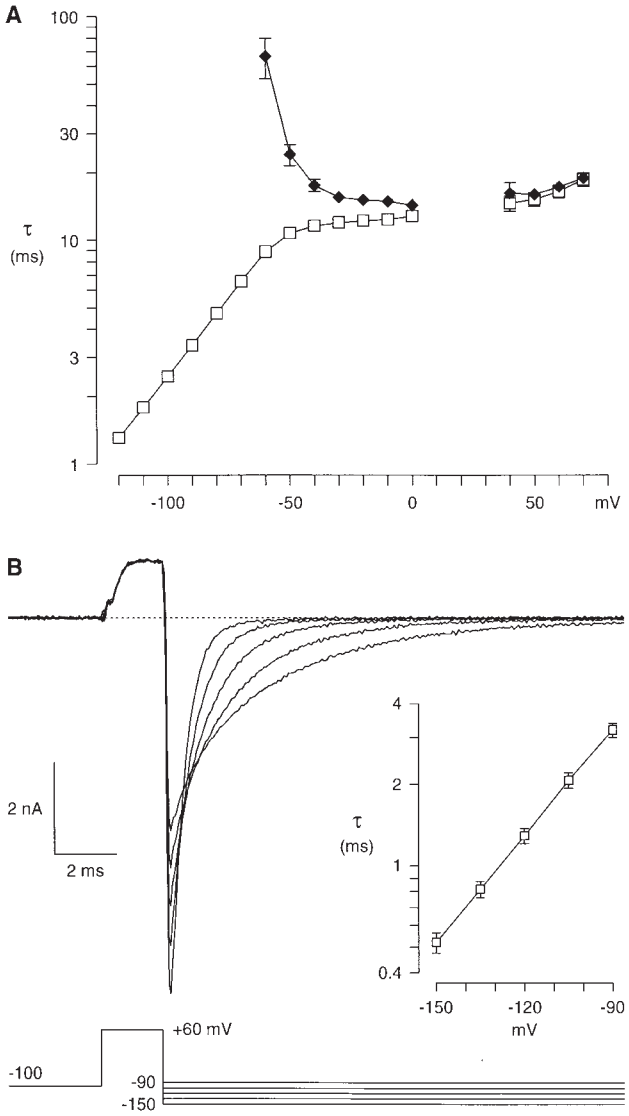

Figure 5. Time course of inactivation and deactivation. (A) Time constants are from single exponential fits, from two protocols. The diamonds are for currents recorded during direct depolarizations (the protocol of Fig. 1), with the fit beginning well after the point of peak inward current, and ending at 60 or 120 ms. The squares are for currents recorded after repolarization from +60 mV (the protocol of Fig. 3), fitted from 0.4–0.6 ms after repolarization to the end of the 40-ms steps. Data are from the same eight cells as Fig. 3 B. (B) Deactivation kinetics at strongly hyperpolarized voltages. Voltage steps were in 15-mV increments, from −90 to −150 mV. The records are from cell a8o29, with 5 kHz Gaussian filtering. The inset shows the time constants, which changed e-fold for 32.8 ± 0.4 mV ($n = 3$).

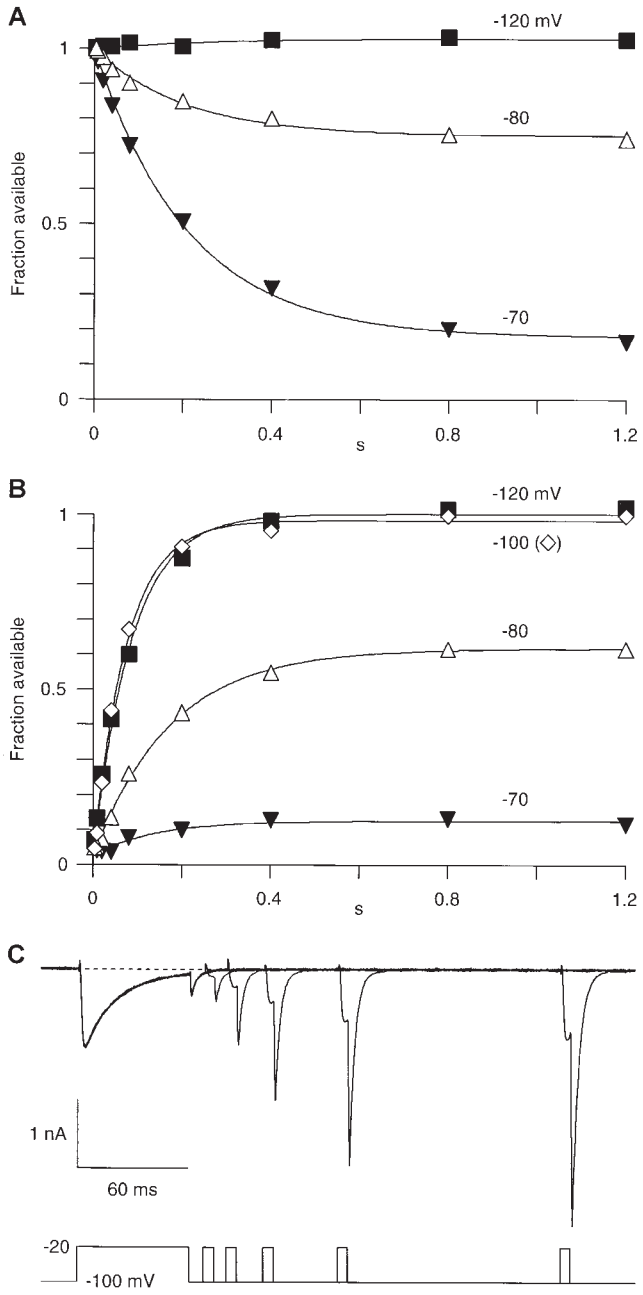

Figure 6. Time course of inactivation and recovery. (A) Effect of prepulses of variable voltage and duration on the current evoked by a test pulse to −20 mV. The currents were normalized to that observed during a test pulse given alone (with no prepulse). The smooth curves are exponential functions, with time constants of 202 ms at −80 mV, and 210 ms at −70 mV. (B) The time course of recovery from inactivation, after 60-ms pulses to −20 mV. The values are the current during the test pulse to −20 mV, divided by the current at the corresponding time in the 60-ms prepulse. Time constants for recovery were 86 ms at −120 mV, 74 ms at −100 mV, and 175 ms at −80 mV. (C) The protocol for recovery from inactivation. Records (analogue filtering at 1 kHz) are shown for recovery at the holding potential of −100 mV, with recovery intervals of 8, 20, 40, 80, and 200 ms. All data in this figure are from cell a8612.

TABLE I

Voltage Dependence of Recovery from Inactivation

Voltage	Open-state inactivation (60 ms, −20 mV)		Closed-state inactivation (600 ms, −70 mV)		Model
mV	*τ (ms)*	*n*	*τ (ms)*	*n*	*τ (ms)*
−120	90 ± 6	7	125 ± 9	7	90
−100	84 ± 9	7	119 ± 12	5	119
−90	151 ± 30	5	150 ± 25	3	162
−80	169 ± 13	8	250 ± 30	5	182

Experimental values are from the protocol of Fig. 6 C ("Open-state inactivation") or Fig. 10 ("Closed-state inactivation"). Approximately 60% of the inactivation at −70 mV is from closed states (Fig. 9). For the model (Fig. 14 A), values are from single exponential fits (using Clampfit) to the time course of the simulated change in P_I after steady state inactivation at 0 mV.

ties of steady state inactivation, voltage steps lasting 1 s were given either directly from −100 mV, or after 60-ms steps to −20 mV to inactivate most of the channels (Fig. 7). At steady state, the measured channel availability should depend only on the tested voltage, i.e., the channel should have "forgotten" whether the inactivating pulse to −20 mV had been given. This comparison can only be done in a narrow voltage range, near the midpoint of the steady state inactivation curve, where the amplitudes of inactivation and recovery are both measurable. The two protocols gave almost identical availability curves: $V_{1/2}$ = −82 ± 2 mV, e-fold for 5.3 ± 0.5 mV, amplitude 1.05 ± 0.02 (inactivation); $V_{1/2}$ = −83 ± 2 mV, e-fold for 4.8 ± 0.1 mV, amplitude 1.06 ± 0.02 (recovery) (n = 6). When the voltage steps lasted <1 s, the measured $V_{1/2}$ was more negative for the recovery protocol than for inactivation, demonstrating that steady state had not been reached (data not shown).

The time course of inactivation and recovery showed no clear deviation from exponential kinetics for steps lasting up to ~1 s (Fig. 6 A). This is consistent with the existence of a single inactivation process for α1G in that time scale. It is possible that separate slow inactivation processes occur in the second-to-minute time scale, as reported for many voltage-dependent channels, so the "steady state" inactivation curve reported here pertains only to the primary "fast" inactivation process.

Completeness of Inactivation

The inactivation curve could be described well by a single Boltzmann relation, assuming that channels inactivate fully at depolarized voltages (Fig. 7). The currents recorded during depolarizations do decay to near zero, but small currents are consistently observed at the end of the pulse (Fig. 1 A). This was observed even after depolarizations lasting 120 ms (Fig. 8 A). If the inactivated state is fully absorbing, only 0.0003 of the channels should remain open after 120 ms (assuming that the current decays toward zero with τ = 15 ms), but the

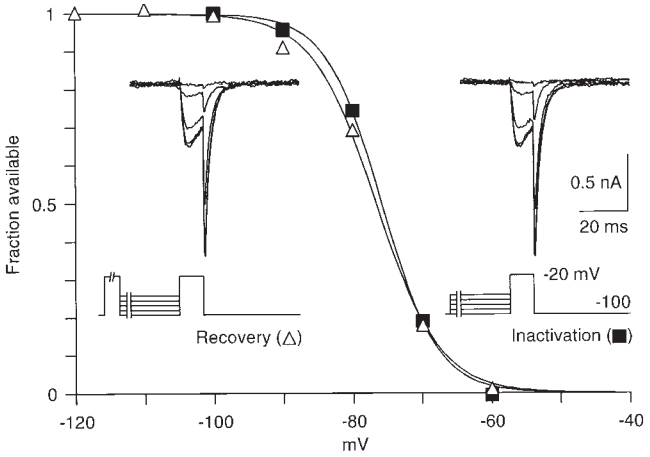

Figure 7. Voltage dependence of steady state inactivation. Steps lasting 1 s to the indicated voltages were followed by 5-ms test pulses to −20 mV. The protocol was run either with no preceding depolarization (for inactivation) or immediately after a 60-ms step to −20 mV (for recovery). For the recovery protocol, the values are the ratio of current in the test pulse to the current during the 60-ms prepulse, measured at comparable times. For the inactivation protocol, currents were normalized to the value at −100 mV (i.e., with no prepulse). Test pulses (with no prepulse) were given before and after the rest of the protocol, to control for rundown or accumulation of inactivation. The smooth curves are fits to a Boltzmann relation, with $V_{1/2} = -76$ mV, e-fold for 4.0 mV (inactivation) and $V_{1/2} = -77$ mV, e-fold for 4.5 mV (recovery). Cell a8n02, 1 kHz analogue antialias filtering.

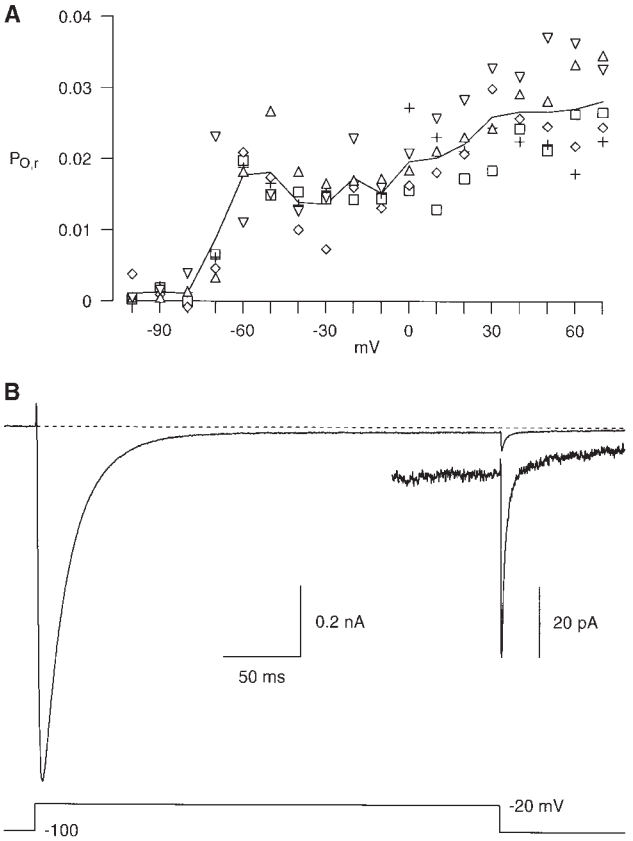

Figure 8. Test for window current. (A) Incomplete inactivation after 120-ms depolarizations. Tail currents at −100 mV were fitted to a single exponential (plus a constant) beginning 0.6–0.8 ms after repolarization from the voltages indicated (protocol of Fig. 1, except voltage steps lasted 120 ms). $P_{O,r}$ was calculated by dividing the initial tail current amplitude (sum of the exponentially decaying component, plus the constant) by the instantaneous current at −100 mV after a 2-ms depolarization to +60 mV (the protocol of Fig. 3). Each symbol is a different cell ($n = 5$), and the line is drawn through the mean values. (B) Incomplete inactivation for 300-ms depolarizations to −20 mV. The records are the averaged currents from four depolarizations, in each of five cells. The inset shows the current at the end of the step and the tail current, at a 10× higher amplification. 1 kHz Gaussian filter.

peak tail current amplitudes correspond to $P_{O,r} \sim 0.02$ over a wide voltage range (−60 to +70 mV). The tail currents were small and noisy, so the measured current amplitudes show considerable variability, but residual channel activation was clearly detectable.

The completeness of inactivation was evaluated further using longer (300-ms) depolarizations (Fig. 8 B). The averaged record shows a small steady state current at −20 mV, followed by a tail current with a fast component appropriate for channel closing at −100 mV. For the five cells included in that record, from a single exponential fit to the first ~30 ms of the tail current, $\tau = 2.7 \pm 0.5$ ms with amplitude 57 ± 11 pA (with an offset of 10 ± 2 pA, discussed below). The $P_{O,r}$ at the peak of the tail current was 0.0118 ± 0.0004 ($n = 4$). The $P_{O,r}$ estimated from the current at the end of the step to −20 mV was comparable (0.013 ± 0.002, $n = 4$). These results suggest that inactivation of α1G is strong but only ~99% complete, at least for depolarizations up to 300 ms.

Another possible source of incomplete inactivation is a "window current" produced by overlap of the steady state activation and inactivation curves. Roughly speaking, that current should be maximal halfway between the midpoint voltages of the two curves (approximately −70 mV for α1G). Tail currents after 600-ms pulses to −70 mV were very small (12 ± 5 pA at −100 mV, $n =$ 6), corresponding to a $P_{O,r}$ of ~0.003, suggesting little steady state activation at −70 mV.

As noted above, single exponential fits to tail currents from the protocol of Fig. 8 B yielded an apparently nondeactivating component of 10 ± 2 pA, which corresponds to $P_{O,r} = 0.002$. (Fits to two exponentials gave a slow component of 12 ± 3 pA, $\tau = 52 \pm 12$ ms, with an offset of 4 ± 1 pA, $n = 5$.) One possible interpretation is that the slow component is a "resurgent current," reflecting channels recovering from inactivation by passing through the open state (Raman and Bean, 1997).

For comparison, we calculated the resurgent current expected if all of the channels must recover through

the open state. We used a three-state scheme: C ← O ↔ I, assuming that channel closing is irreversible at −100 mV. The inactivation (k_I) and recovery (k_{-I}) rates can be estimated from the limiting time constants for inactivation (τ = 15 ms) and recovery (τ = 100 ms): k_{-I} = 1/100 = 0.01 ms^{-1}, and k_I = 1/15 − k_{-I} = 0.057 ms^{-1}. From the tail current time constant at −100 mV (τ = 2.5 ms), the channel closing rate k_C = 1/2.5 − k_I = 0.34 ms^{-1}. From the analytic solution to the general three-state model (Gutnick et al., 1989), those values predict a reopening current with peak P_O = 0.023 (at 9.8 ms, decaying with τ = 117 ms), starting from the initial condition P_I = 1. Thus, the observed $P_{O,r}$ of 0.002 is consistent with ~8% of the channels recovering through the open state. Since the slow component of the tail current could be explained in other ways (e.g., a small amount of slow deactivation), this value should be considered an upper limit for the fraction of channels that recover through the open state.

Another argument that inactivation and activation are not strictly coupled is that a C … C ↔ O ↔ I scheme predicts much less complete inactivation than observed. If the rate constants for inactivation and recovery are truly voltage independent with the values estimated above, $P_I = k_I/(k_I + k_{-I})$ = 0.85 at steady state (at depolarized voltages where the C ↔ O reaction favors the open state). This is additional evidence that recovery from inactivation cannot occur primarily through the open state; i.e., the limiting rate for recovery from inactivation is considerably faster than the rate constant for the O ← I reaction.

Closed-state Inactivation

Fig. 7 demonstrates that there is considerable inactivation at quite negative voltages, below the range where channel activation is detectable (see Fig. 1 B and Fig. 4). This observation suggests that channels can inactivate directly from closed states. However, it is possible that open-state inactivation could slowly accumulate even if P_O is low, perhaps undetectably low. To examine this quantitatively, we calculated the amount of inactivation expected if channels can inactivate only from the open state. That can be done in a model-independent manner, if we make two assumptions: (a) the microscopic rate constant for inactivation k_I (O → I) is the reciprocal of the nearly voltage-independent time constant measured at more than −30 mV, and (b) recovery from inactivation can be neglected (i.e., inactivation is absorbing). We do not mean to imply that these assumptions are true, but they allow simple calculation of the amount of inactivation expected to be produced by a voltage protocol, and deviations from the "predicted" inactivation are likely to be informative.

The predicted inactivation was calculated as follows: first, after measuring the instantaneous I–V relation for a cell (Fig. 3 B), currents are converted to relative P_O values ($P_{O,r}$), by dividing the observed current by the instantaneous current at the same voltage. This gives $P_{O,r}$ as a function of time (relative to that at +60 mV). The expected open-state inactivation is then calculated by integrating $dP_I/dt = k_I P_{O,r}$. That is calculated as the point-by-point sum

$$P_I = \Sigma k_I P_{O,r}(t)\Delta t \quad (1)$$

during the protocol. Note that this calculation does not make any assumptions about the kinetic scheme for channel activation; i.e., it is independent of number and arrangement of closed states. Similar analyses have been done by Bean (1981) for Na^+ channels, and Herrington and Lingle (1992) for T-channels of GH_3 cells.

At −70 mV, where channel opening was clearly detectable, the observed inactivation was approximately twice the predicted value (Fig. 9 A). The difference was larger at −80 mV (Fig. 9 B), where inward currents were visible in one or two of the four cells analyzed. If recovery from inactivation were considered, the predicted inactivation would be reduced further, increasing the discrepancy. We conclude that there is excess inactivation that cannot be accounted for by inactivation from the open state, presumably indicating inactivation directly from closed states.

To determine whether inactivation from closed states is a fundamentally different kinetic process from open-state inactivation, we examined recovery from inactivation after 600-ms steps to −70 mV (Fig. 10). Recovery from inactivation was similar, whether inactivation was produced primarily from open or closed states (Table I). Notably, there was little voltage dependence to recovery (varying approximately twofold from −120 to −80 mV), and recovery could be quite rapid ($\tau \sim$ 100 ms at −120 mV). These results suggest that the inactivated states reached from open and closed states interconvert rapidly. Alternatively, it is possible that a single inactivated state is accessed from both open and closed states.

Open-state Inactivation

The results described above demonstrate that inactivation can occur from closed states, at least for long, weak depolarizations to voltages near the midpoint of the inactivation curve. But what about brief, strong depolarizations? Fig. 11 compares the measured and predicted open-state inactivation produced by the protocol of Fig. 3. (Inactivation was measured from an additional test pulse to +60 mV, given 20 ms after each record; see Fig. 11, inset.) At negative potentials, there is a good match between measured and predicted inactivation. At positive potentials, the predicted inactivation is larger, possibly due to the observed tendency of inacti-

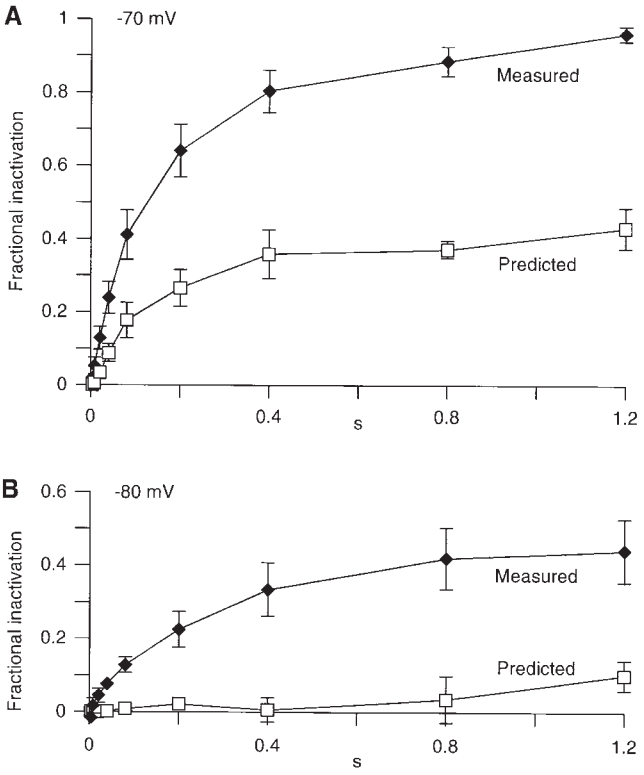

Figure 9. Test for closed-state inactivation. Voltage steps to −70 mV (A) or −80 mV (B) for the indicated duration were immediately followed by 5-ms test pulses to −20 mV. Inactivation measured from the test pulses (diamonds) is compared with the expected open-state inactivation (squares) calculated from the integrated current during the step to −70 mV (Eq. 1). $n = 3$ (A), $n = 4$ (B).

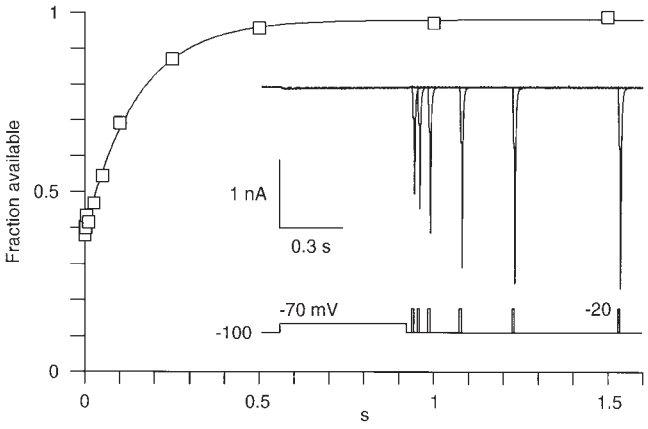

Figure 10. Recovery from closed-state inactivation. In this cell, a 600-ms step to −70 mV produced a small inward current (calculated $P_{O,r} = 0.004$ at peak), but a subsequent 10-ms test pulse to −20 mV demonstrated 40% inactivation (compared with 8% predicted open-state inactivation). The main figure shows the time course of recovery from inactivation at −100 mV, fitted to an exponential function with $\tau = 149$ ms. Currents were measured during the steps to −20 mV, and were normalized to the current recorded during test pulses to −20 mV (with no prepulse to −70 mV) given after the protocol. The inset shows records for recovery intervals of 25, 50, 100, 250, 500, and 1,000 ms (cell d8o28, 500 Hz Gaussian filter). In this cell, the peak $P_{O,r}$ and the amount of inactivation at −70 mV were both less than typically observed (compare with Figs. 6, 7, and 9).

vation to slow slightly at positive voltages, or to some amount of recovery from inactivation.

Most of the inactivation observed at −120 to −100 mV in Fig. 11 can be attributed to the predicted open-state inactivation produced during the initial 2-ms step to +60 mV (0.15 ± 0.04, $n = 5$). But the amount of inactivation increases with depolarization from −90 to −60 mV, and that extra inactivation can be quantitatively explained by inactivation from the open state during the tail current. That is, a fraction of channels inactivate after repolarization, rather than closing. This behavior is expected from inactivation that is state but not voltage dependent, as channels have a "choice" of pathways for leaving the open state (C … C ← O → I). In contrast, with a model where inactivation and recovery are intrinsically voltage dependent, channels would begin to recover from inactivation immediately upon repolarization.

Cumulative Inactivation

State-dependent inactivation is often associated with cumulative inactivation, a phenomenon where repetitive pulses produce significant inactivation, even when little or no inactivation is visible during each depolarization (Neher and Lux, 1971; Aldrich, 1981). We do observe strong cumulative inactivation for brief trains of pulses for α1G, either using square voltage steps (Fig. 12 A) or action potential–like depolarizations (Fig. 12 B).

Cumulative inactivation results from "hidden" inactivation, which can occur either "on the way up" (during activation, before the point of peak current), or "on the way down" (during the tail current). Inactivation "on the way up" is favored if inactivation occurs primarily from intermediate closed states (Aldrich, 1981; Klemic et al., 1998), while inactivation occurs from open states "on the way down" if channel deactivation is slow (DeCoursey, 1990). As might be expected for slowly deactivating T-channels, the cumulative inactivation in Fig. 12 A can be accounted for by open-state inactivation, with much of the predicted inactivation occurring during the tail currents (see lower trace). The actual measured current amplitudes at the end of the second to fourth pulses were 51 ± 2, 31 ± 2, and 21 ± 2% of the first pulse current, comparable to the predicted inactivation of 58 ± 2, 36 ± 3, and 22 ± 4% ($n = 5$).

Another sign of state-dependent inactivation is "nonmonotonic recovery from inactivation" (Neher and Lux, 1971; Marom and Levitan, 1994). For pairs of brief depolarizations, channels continue to inactivate during the initial part of the interpulse interval, before recovery from inactivation begins, producing a U-shaped

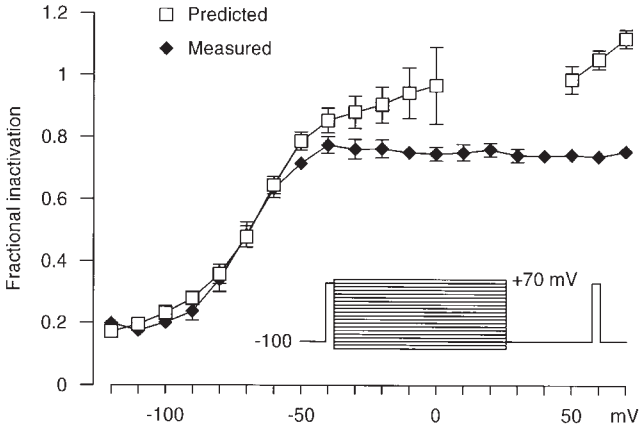

Figure 11. Predicted open-state inactivation. The voltage protocol is shown in the inset. The steps to +60 mV lasted 2 ms each, the variable steps were 40 ms, and the interval at −100 mV was 20 ms. Measured inactivation is from the currents during the two steps to +60 mV ($1.0 - I_{+60,post}/I_{+60,pre}$). Predicted inactivation was calculated from Eq. 1, including the $P_{O,r}$ values from all three voltage levels before the final test pulse to +60 mV.

time course for the current measured during the second pulse (Fig. 13). However, apparent nonmonotonic recovery can be observed for interpulse intervals that are not long enough to fully close the channel, if that leads to more channel activation during the second pulse (Gillespie and Meves, 1980). That is, a larger test pulse current could result from greater channel activation, rather than less inactivation, for very brief intervals. To exclude this possibility, we delivered a third pulse, after allowing 20 ms for complete channel closing. Currents during the third pulse also showed a U-shaped time dependence (Fig. 13), although inactivation during the 20-ms tail current (and at early times during the third pulse) made the U shape less dramatic. Since nonmonotonic recovery would not occur at all if inactivation were strictly voltage dependent, this is good evidence for state-dependent inactivation.

Kinetic Model

A model for channel gating can be useful both as an empirical description and as a testable hypothesis for the underlying mechanism. We wanted to develop a model that could reproduce the major experimental results of this study: inactivation is state dependent, fastest from open states, but detectable from closed states. Deactivation is strongly voltage dependent, compared with channel opening (measured as time to peak). Inactivation is strong, but there is a sustained current, corresponding to a $P_{O,r}$ of 1–2%, over a wide voltage range. Inactivation and recovery reach voltage-independent limiting rates. Repetitive depolarizations produce cumulative inactivation, but inactivation is stronger during a single maintained depolarization.

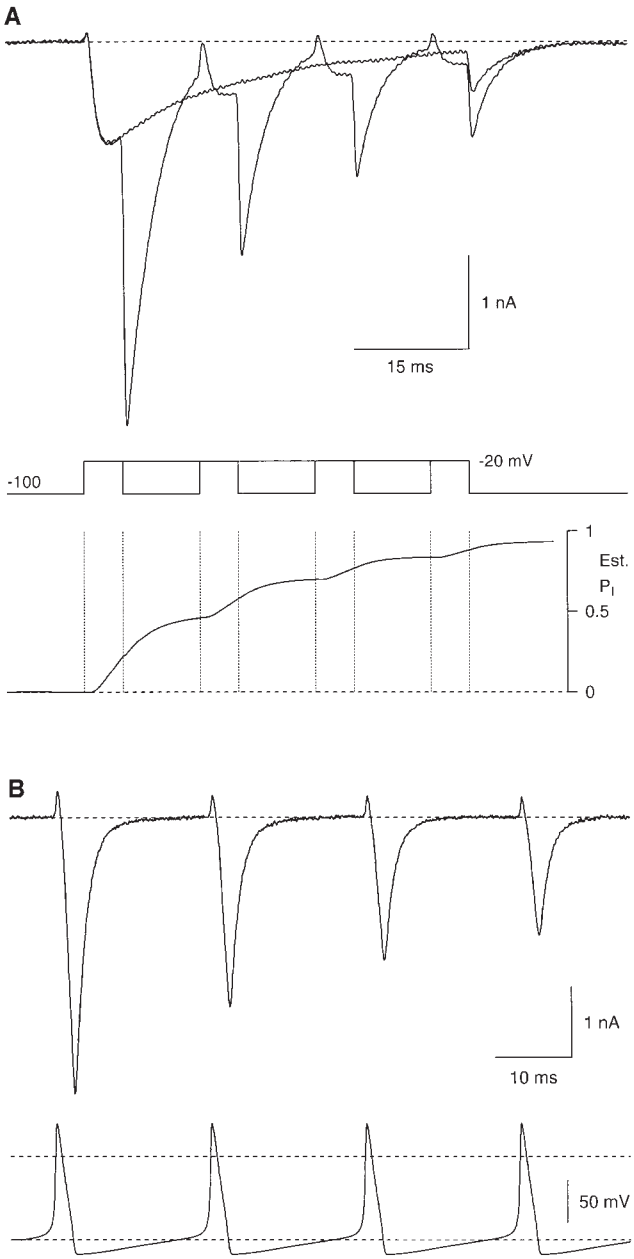

Figure 12. Cumulative inactivation. (A) The upper panel is two superimposed current records, a single 50-ms depolarization to −20 mV, and four steps to −20 mV for 5 ms each, separated by 10-ms intervals at −100 mV. The lower panel is the predicted open-state inactivation for the four-pulse protocol. Cell a8612, 2 kHz Gaussian filter. (B) Inactivation during a train of four action potential–like depolarizations. Cell e8612, 5 kHz Gaussian filter. The voltage command (shown below) was simulated from the Hodgkin-Huxley (1952b) model for the squid axon, modified to allow spontaneous 50-Hz repetitive firing by shifting the voltage dependence of the "m" gate by 2 mV to more negative voltages. The action potentials were scaled to an initial voltage of −100 mV, with an overshoot of +39 mV. The dashed lines are at 0 and −100 mV.

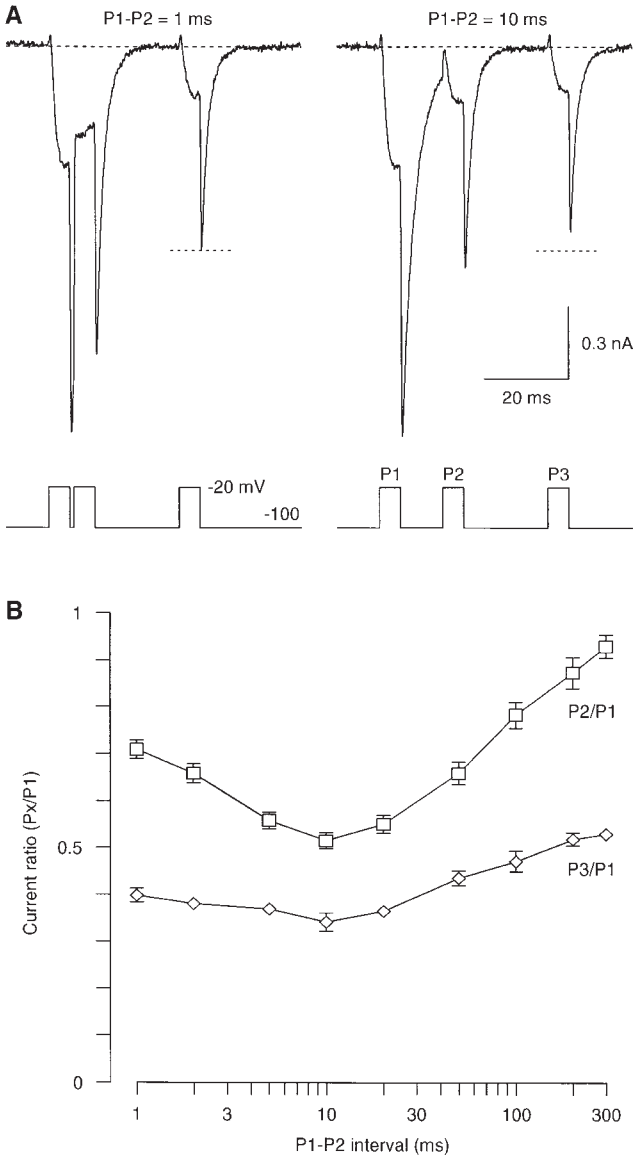

Figure 13. Nonmonotonic recovery from inactivation. Three pulses were given (each 5 ms to −20 mV), with a variable interval (1–300 ms) between the first two pulses (P1 and P2), and 20 ms between P2 and P3. (A) Sample records for P1–P2 intervals of 1 and 10 ms. Note that the 1-ms interval at −100 mV is not long enough for many channels to close. The P2 current is clearly larger for the 1-ms interval, and the P3 current is slightly larger (easiest to see in the tail current amplitudes following P3, see dashed lines). Cell a8702, 3 kHz Gaussian filter. (B) The time course of recovery from inactivation, averaged from seven cells. Note the log time scale. The decrease in P2 amplitude from 1 to 10 ms could reflect either continued inactivation during the tail current, or residual activation remaining from P1 (see A). But the 20-ms P2–P3 interval is long enough for channels to fully deactivate, so the decrease in P3 amplitude from 1 to 10 ms indicates a genuinely nonmonotonic time course for recovery from inactivation.

We considered a model where inactivation is coupled allosterically to voltage sensor activation (Fig. 14 A), which has proven successful for describing inactivation for several voltage-dependent channels (Kuo and Bean, 1994; Klemic et al., 1998; Patil et al., 1998). The model involves sequential activation of four voltage sensors (presumably the S4 regions), followed by a distinct channel opening step with less voltage dependence. This can describe the observed delay before channel opening, but voltage-independent channel opening (k_O) limits the voltage dependence of the time to peak. Channel closing (k_{-O}) must have significant voltage dependence, however, to produce the observed exponential voltage dependence of deactivation (Fig. 5 A). Inactivation is allowed from any of the closed or open states, as in the Hodgkin and Huxley (1952b) Na^+ channel model, but channel activation favors inactivation (and slows recovery). The rate constants for inactivation and recovery are state dependent, but do not depend directly on voltage.

We began by assuming that all four voltage sensors are allosterically coupled to inactivation. Simulations initially appeared to be successful, but close examination revealed an interesting discrepancy. At voltages near the threshold for significant activation, the sustained current was larger than observed experimentally. Although the true steady state P_O did increase monotonically with depolarization, after depolarizations producing partial inactivation (e.g., 60–120 ms), the simulated tail currents were approximately twice as large at near-threshold negative voltages than at positive voltages. This was not seen experimentally (Fig. 8 A; even more clear for 60-ms depolarizations, where the tail currents were larger and more easily measurable; data not shown). In fact, although the characteristic "crossover" (Randall and Tsien, 1997) of T-current records was clear in the current–voltage curve (Fig. 1 A), it was barely detectable when the experimental records were converted to P_O (Fig. 14 B). This occurred even though the measured time constants for macroscopic inactivation were slower at more negative voltages (Fig. 5 A), as expected when slow, rate-limiting channel opening is followed by relatively fast inactivation.

The crossover exhibited by the simulations suggested that the model underestimated the rate of inactivation at more negative voltages, which presumably must occur from closed states. We thus modified the scheme, so that activation of only the first three voltage sensors affects the inactivation rate. That is, the last voltage sensor to move (C_3–C_4) has no further effect on the inactivation rate, and the open channel inactivates at the same rate as closed channels in C_3 and C_4. This is arbitrary, but there is precedent for differential coupling of voltage sensors to inactivation of Na^+ channels (Mitrovic et al., 1998). Faster inactivation from the intermedi-

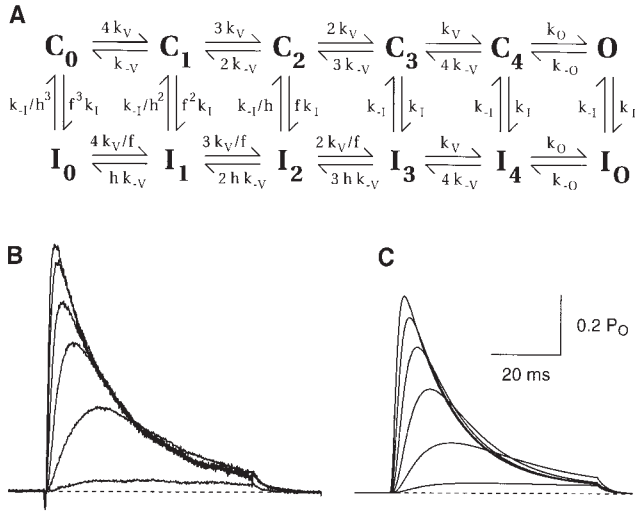

Figure 14. A kinetic scheme for gating of α1G T-channels. It differs from Kuo and Bean (1994) and Klemic et al. (1998) in assuming that the rates for inactivation and recovery are the same for the rightmost three states (C_3, C_4, and O). The model includes six rate constants at 0 mV, for voltage sensor movement (k_V = 2,500 s^{-1}, k_{-V} = 8 s^{-1}), channel opening/closing (k_O = 4,000 s^{-1}, k_{-O} = 25 s^{-1}), and inactivation (k_I = 70 s^{-1}, k_{-I} = 1.4 s^{-1}). Three of the rate constants (k_V, k_{-V}, and k_{-O}) depend exponentially on voltage, changing e-fold for 25, −18, and −34 mV depolarization (respectively). Inactivation is allosterically coupled to movement of the first three voltage sensors, with factors f = 0.2 for inactivation rate constants and h = 0.5 for recovery. (B) Records of $P_{O,r}$ versus time, from −70 to −20 mV, calculated by dividing currents (recorded by the protocol of Fig. 1 A) by the peak tail current amplitude at each voltage (protocol of Fig. 3). Cell a8612, 3 kHz Gaussian filter. (C) Simulated P_O versus time records. The scale bars apply to both B and C.

ate closed state C_3 significantly reduced the sustained current at negative voltages, and reduced the crossover (Fig. 14 C). Allowing only the first two voltage sensors to affect the inactivation rate eliminated crossover of P_O records, but degraded the quality of the fit in other ways, notably weakening the voltage dependence of steady state inactivation.

The scheme of Fig. 14 A can accurately describe many aspects of the experimental data (Fig. 15). Current records cross over at negative voltages (Fig. 15 A) and activate in the appropriate voltage range (Fig. 15, B and C). The sum of two Boltzmann distributions was required for accurate description of the simulated activation curve (Fig. 15 C; compare with Fig. 4 A). The voltage dependence of the time to peak (Fig. 15 D) resembled the experimental data (Fig. 4 B), approaching 1 ms at strongly positive voltages. Tail currents from the protocol of Fig. 3 A decayed nearly monoexponentially (Fig. 15, E and F), although the model does not describe the small increase in time constant at positive voltages (Fig. 5 A). The model reproduces cumulative inactivation (Fig. 15 G), with considerable inactivation occurring

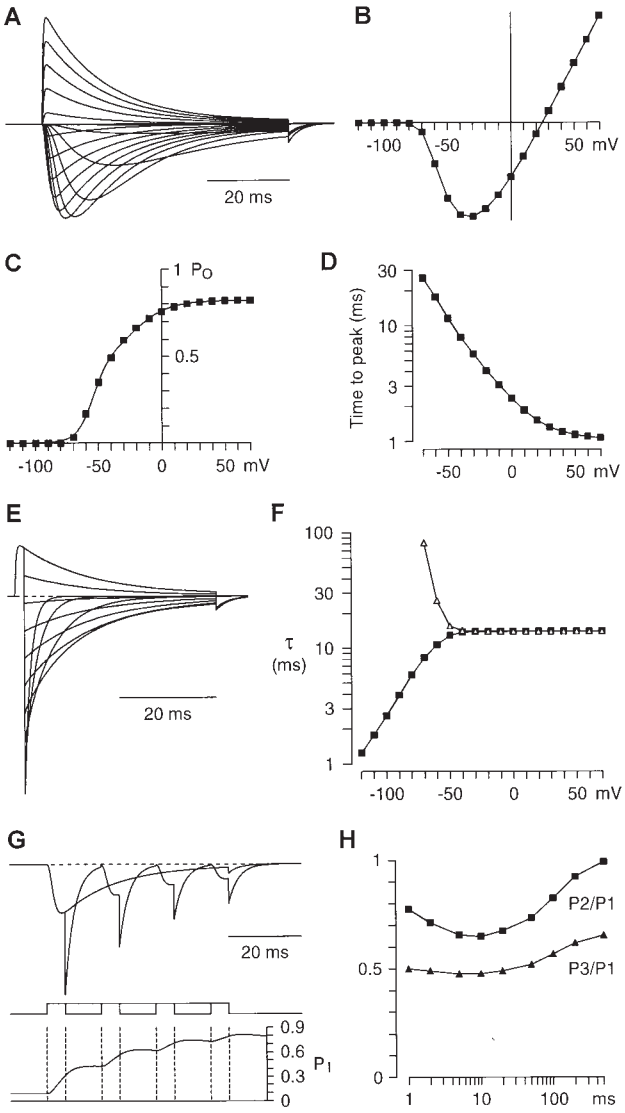

Figure 15. Simulation of α1G T-currents. Parameters are given in the legend to Fig. 14. Currents were calculated assuming a reversal potential of +25 mV, with a linear open-channel I–V. (A) Currents during 60-ms depolarizations from −100 mV to voltages from −90 to +70 mV, as in Fig. 1 A. Peak current–voltage relations (B), the peak probability that the channel is open (C), and the time to peak (D) from the protocol of A (compare with Fig. 1 B and Fig. 4, A and B, respectively). The smooth curve in C is the sum of two Boltzmann functions: $V_{1/2}$ = −54 mV, e-fold for 6.3 mV, amplitude 0.46; $V_{1/2}$ = −23 mV, e-fold for 13.9 mV, amplitude 0.36. (E) Currents from the protocol of Fig. 3, recorded in 20-mV increments from −120 to +60 mV, after 2-ms depolarizations to +60 mV. (F) Time constants for inactivation (triangles) from A, and for inactivation plus deactivation (squares) from E, shown as in Fig. 5 A. Time constants changed e-fold for 26 mV from −70 to −120 mV. (G) Currents during a train of 5-ms depolarizations from −100 to −20 mV, given at 15-ms intervals, superimposed on the current during a 50-ms depolarization to −20 mV. The lower panel shows the summed probability of being in an inactivated state, in response to the four depolarizations shown above. Compare with Fig. 12. Note that net inactivation occurs during the tail current after the first two steps, despite some recovery from inactivation (more apparent after the last two steps). (H) Nonmonotonic recovery from inactivation, using the protocol of Fig. 13.

during tail currents. Nonmonotonic recovery from inactivation occurs after brief (5-ms) steps, although this is barely visible in the P3/P1 ratio (Fig. 15 H).

It is noteworthy that the tail currents could be described by single exponentials (Fig. 15, E and F), even in the intermediate voltage range (near −60 mV) where some channels inactivate and others deactivate. If both processes were effectively irreversible, a single exponential would result ($1/\tau = k_C + k_I$; see Cota and Armstrong, 1989), but activation is not negligible near −60 mV. In fact, some parameter sets did give clearly biexponential tail currents (especially if C–C kinetics were fast). In the experimental data, a very rapid component was occasionally visible, possibly an off-gating current, but there was no evidence for separate components corresponding to deactivation and inactivation. In principle, for a 12-state kinetic scheme, the macroscopic currents include 11 exponential components, but it is not unusual to find that a single exponential can give a good operational description under some conditions.

The model also produced appropriate steady state inactivation, including its steep voltage dependence ($V_{1/2}$ = −81 mV, e-fold for 5.0 mV). Inactivation near the $V_{1/2}$ was predominantly from closed states. Recovery from inactivation was weakly voltage dependent (Table I). There was no obvious resurgent current during recovery from inactivation, but the tail current (primarily reflecting deactivation of the small steady state current) was ~20% slower than after brief depolarizations, reflecting some channels recovering from inactivation through the open state (simulations not shown).

discussion

Functional expression of the α1G clone in HEK 293 cells produced currents with the essential kinetic properties of T-type calcium currents. Specifically, the voltage dependence of activation ($V_{1/2} \sim -50$ mV) is clearly in the LVA range, and inactivation ($V_{1/2} \sim -80$ mV) also occurs at more negative voltages than for most HVA channels. Inactivation is not only rapid ($\tau \sim$ 15 ms at −40 mV and above), but also nearly complete. α1G deactivates ~10-fold slower than HVA channels (τ = 2.5 ms at −100 mV). Similar properties have been observed for α1G expressed in *Xenopus* oocytes (Perez-Reyes et al., 1998), but use of a mammalian cell line allowed control of the intracellular medium, so that currents could be studied in nearly physiological conditions. The kinetic analysis in this study depended on the ability to isolate α1G currents over a wide voltage range, without detectable contamination from other currents, as shown by the envelope test (Fig. 2) and the absence of ionic currents at the observed reversal potential (Fig. 3 A).

State Dependence of Inactivation

The main goal of this study was to characterize the kinetics of inactivation in α1G channels. We conclude that inactivation is state dependent, with little intrinsic voltage dependence. For brief strong depolarizations, inactivation occurs primarily from the open state, but long weak depolarizations produce inactivation from partially activated closed states. We will next discuss the evidence for these conclusions.

The macroscopic inactivation and recovery processes reach essentially voltage-independent time constants at extreme voltages, above −50 mV for inactivation and below −90 mV for recovery (Figs. 5 and 7). This can be described by intrinsically voltage-dependent inactivation, if rate constants depend nonexponentially on voltage, as for β_h in the original Hodgkin and Huxley (1952b) model, but a voltage-independent rate-limiting step is a more attractive explanation. Furthermore, open-state inactivation at a voltage-independent rate can account for the inactivation observed for brief depolarizations and the subsequent tail currents (Fig. 11). Most notably, there was more inactivation during tail currents at −80 to −60 mV than at more negative voltages, as predicted by open-state inactivation, since channels deactivate slowly in that range. The observation of nonmonotonic recovery from inactivation (Fig. 13) confirms that inactivation can continue to occur after repolarization, as expected for state-dependent but not voltage-dependent inactivation.

Although open-state inactivation can account for the effects of brief depolarization (Fig. 11), inactivation also occurred slowly during depolarizations to −90 mV (Fig. 7), where no channel opening was detectable. At −70 or −80 mV, the amount of observed inactivation considerably exceeded that predicted by voltage-independent open-state inactivation (Fig. 9). Unless the rate for open-state inactivation increases more than twofold at these hyperpolarized voltages, which is unlikely, inactivation must also occur from closed states. The simplest explanation for the inactivation observed below −60 mV is that activation of voltage sensors favors inactivation, even if the channel does not open (Fig. 14 A). For α1G, inactivation is faster from the open state than from some of the intermediate closed states, since macroscopic inactivation slowed below −40 mV, and a maintained depolarization produced more inactivation than repetitive pulses (Fig. 13 A).

Open- and closed-state inactivation of α1G appear to be closely linked processes, since recovery from inactivation is similar after procedures that favor open-state inactivation (60-ms pulses to −20 mV) or closed-state inactivation (600-ms pulses to −70 mV). The absence of a significant inward current during recovery from inactivation (Fig. 8) demonstrates that the primary pathway for recovery from inactivation is via closed states.

It is possible that what we describe as open-state inactivation actually occurs from a closed state that is in rapid, voltage-independent equilibrium with the open state (Marom and Levitan, 1994). Since this can be difficult to distinguish from inactivation directly from the open state, even with single channel data, we retain the expression "open-state inactivation" to emphasize that this form of inactivation is closely coupled kinetically to channel opening. Although our model assumes that inactivation occurs at the same rate from certain closed states (C_3 and C_4) as from the open state, open-state inactivation is the predominant pathway except at the most negative voltages, mainly because the $C_4 \leftrightarrow O$ equilibrium is strongly to the right for the parameters used, so occupancy of C_3 and C_4 is generally low.

Although our model describes well many qualitative and quantitative features of the experimental data, it should be considered preliminary. The model parameters were found by trial and error, rather than rigorous parameter estimation procedures based on quantitative error minimization. We have not systematically tested alternative models. Our data do not include information from single-channel or gating current experiments, which have proven important for modeling gating of other channels. We believe it is useful to present this model at this time, as a possible basis for future studies on the gating of both cloned and native T-channels.

Comparison with Native T-currents

α1G is likely to underlie native T-currents in some but not all cells. Notably, it is highly expressed in the thalamus (Perez-Reyes et al., 1998). Two other α1 subunits (α1H and α1I) produce T-currents in expression systems (Cribbs et al., 1998; Perez-Reyes et al., 1998; Lee et al., 1999), and the existence of additional α1 genes cannot be excluded. Other sources of diversity in channel properties, including accessory subunits and post-translational modifications, remain to be fully explored for T-channels. It has been suggested that α_1 subunits normally associated with HVA channels can produce T-like activity under some conditions (Soong et al., 1993; Meir and Dolphin, 1998), but the cloning of three indisputable T-channels makes this possibility less attractive as a general explanation for native T-currents (Randall and Tsien, 1997; Bean and McDonough, 1998; Lambert et al., 1998; Nakashima et al., 1998).

Kinetic and pharmacological diversity among T-channels is well established (Huguenard, 1996). One feature with possible implications for mechanisms of channel gating is the voltage dependence at extreme voltages, which could reveal voltage-independent limiting rates (Chen and Hess, 1990). We found clear evidence for voltage independence of the inactivation process (above −50 mV) and recovery (below −90 mV). This agrees well with some studies (Chen and Hess, 1990; Herrington and Lingle, 1992), although a limiting voltage-independent rate for recovery is not always clear (Huguenard and McCormick, 1992). In contrast, channel deactivation remained strongly voltage dependent even at −150 mV (Herrington and Lingle, 1992; Todorovic and Lingle, 1998; but see Chen and Hess, 1990). We have not examined activation kinetics closely in this study, but channel opening became quite rapid at depolarized voltages, with time to peak 1.4 ± 0.1 ms at +60 mV ($n = 7$).

Our data for α1G are consistent with single exponential kinetics both for development of inactivation and for recovery, on a time scale up to 1 s. This is consistent with most previous work on native T-channels, although some studies have reported multiexponential kinetics (Bossu and Feltz, 1986; Herrington and Lingle, 1992). A preliminary report suggests that α1G may also exhibit a second inactivation process, on a longer time scale (Martin et al., 1998).

Comparison with Inactivation in Other Voltage-dependent Channels

There are some similarities among inactivation processes for different voltage-dependent channels. Fast inactivation of Na^+ channels and N-type inactivation of K^+ channels reach a limiting rate at positive voltages. At intermediate voltages, macroscopic inactivation is voltage dependent due to kinetic coupling to the activation process, which is relatively slow at such voltages. Inactivation is strong but not necessarily 100% complete. Inactivation of α1G channels shares these properties.

One striking difference from Na^+ channels is that recovery from inactivation shows little voltage dependence for T-current (Table I; Chen and Hess, 1990). This suggests a voltage-independent rate-limiting step for recovery, consistent with the view that the microscopic inactivation and recovery rates are both independent of voltage. In one study, recovery became voltage independent for Na^+ channels, but only below −160 mV (Kuo and Bean, 1994). Further work will be necessary to determine whether these differences are merely quantitative, or reflect qualitatively different inactivation mechanisms.

Inactivation of α1G was strong but incomplete, with 98–99% inactivation over a wide voltage range. There is considerable variability in the extent of inactivation of Na^+ channels, 70–97% in the squid giant axon (Vandenberg and Bezanilla, 1991) but 99.9% in mammalian skeletal muscle (Cannon and Corey, 1993). In squid axon, the extent of inactivation decreases with strong depolarization (Chandler and Meves, 1970), which may be true to a lesser extent for α1G (Fig. 8). This effect is not clearly associated with a slower macroscopic inactivation rate in squid axon (Chandler and Meves, 1970), but an ∼20% decrease in the inactivation rate was de-

tectable above +50 mV for α1G (Fig. 5 A). The decreased inactivation with strong depolarization was voltage dependent in squid axon (Bezanilla and Armstrong, 1977), but effects of permeant ions on gating should also be considered for T-channels (Carbone and Lux, 1987; Shuba et al., 1991), since in our ionic conditions the primary charge carriers are Ca^{2+} for inward currents and Na^+ for outward currents.

Fast inactivation of Na^+ and K^+ channels is believed to occur primarily but not exclusively from open states (Bean, 1981; Aldrich and Stevens, 1983; Hoshi et al., 1990), as we find here for α1G. This contrasts with slower inactivation processes of some K^+ (Aldrich, 1981; Klemic et al., 1998, 1999) and HVA Ca^{2+} channels (Patil et al., 1998), where inactivation from closed states appears to be the predominant pathway even at positive voltages.

Possible Physiological Implications

One of the clearest functional roles of native T-channels is generation of the low threshold spike that underlies bursts of action potentials in (e.g.) thalamic relay neurons (Huguenard, 1996). In those cells, T-channels are inactivated at the normal resting potential (near −60 mV). But inactivation can be rapidly removed by hyperpolarizations, such as inhibitory postsynaptic potentials (IPSPs). This allows rebound activation of T-channels and a low threshold spike, terminated in part by T-channel inactivation. The properties of α1G currents are fully consistent with such a scheme.

α1G exhibited a sustained current, with 1–2% of the channels remaining open at all voltages above −70 mV (Fig. 8). Our kinetic model accounts for that current with a finite, voltage-independent rate of recovery from inactivation. This differs from the "window current" predicted from an overlap between the activation and inactivation curves, which has a bell-shaped P_O versus voltage relation (if inactivation is complete at positive voltages, as often assumed), peaking near the foot of the activation curve (Williams et al., 1997). But in either case, there would be a steady state T-current at voltages near the resting potential, which could have interesting consequences for neuronal integration and calcium homeostasis (Williams et al., 1997; Bean and McDonough, 1998). We are not aware of direct evidence for such a current from previous voltage clamp studies of T-current, although current clamp studies on thalamic neurons do suggest existence of a window current (Williams et al., 1997). Our results could overestimate the steady state T-current if additional slow inactivation processes exist, but the time scale we have examined (up to ∼1 s) is sufficient to predict that there should be significant T-channel activity during hyperpolarized intervals during a burst of action potentials.

It is not possible to extrapolate directly from results in an expression system to the situation in vivo, but several kinetic properties of α1G could have important physiological consequences. Activation is quite rapid at positive voltages, so any α1G channels not already activated in a low threshold spike might be activated significantly by a single Na^+-dependent action potential. After repolarization, slow deactivation will keep the channels open for a few milliseconds, producing maintained Ca^{2+} entry (as noted by Huguenard, 1996). In addition, a significant fraction of channels will inactivate (rather than deactivate) after repolarization. This contributes to the strong cumulative inactivation observed for α1G during action potential–like depolarizations (Fig. 13).

The cumulative inactivation critically depends on the state dependence of inactivation, combined with the characteristic slow deactivation of T-channels. Previous models for thalamic T-currents resemble the original Hodgkin and Huxley (1952b) model for Na^+ current, with inactivation depending on voltage but not on the state of activation of the channel. Some degree of cumulative inactivation does occur with Hodgkin-Huxley models, as some channels inactivate without opening in response to brief depolarizations, but recovery from inactivation begins immediately upon repolarization. Correspondingly, the models of Wang et al. (1991) and Huguenard and McCormick (1992) for thalamic T-current produce much less cumulative inactivation than observed here (simulations not shown). It is sometimes assumed that Hodgkin-Huxley models are valid as operational descriptions of macroscopic ionic currents, even if they are not mechanistically correct. However, state-dependent inactivation can produce effects that are not describable by such models, notably in response to repetitive depolarizations (Klemic et al., 1998; Patil et al., 1998). Future studies will be necessary to determine whether T-channels natively expressed in neurons also exhibit strong cumulative inactivation during a burst of action potentials, and to explore the consequences for the role of T-channels in neuronal excitability.

We thank Drs. Leanne L. Cribbs and Toni Schneider for preparation of the α1G cell line, and Dr. Christopher J. Lingle for helpful comments on a draft of this paper.

This work was supported in part by National Institutes of Health grant NS24471 to S.W. Jones and HL58728 to E. Perez-Reyes, and by a Howard Hughes Medical Institute grant to Case Western Reserve University School of Medicine.

Submitted: 3 March 1999 Revised: 19 May 1999 Accepted: 28 May 1999

references

Aldrich, R.W. 1981. Inactivation of voltage-gated delayed potassium current in molluscan neurons. A kinetic model. *Biophys. J.* 36: 519–532.

Aldrich, R.W., and C.F. Stevens. 1983. Inactivation of open and closed sodium channels determined separately. *Cold Spring Harbor Symp. Quant. Biol.* 48:147–153.

Armstrong, C.M., and D.R. Matteson. 1985. Two distinct populations of calcium channels in a clonal line of pituitary cells. *Science.* 227:65–67.

Armstrong, C.M., and F. Bezanilla. 1977. Inactivation of the sodium channel. II. Gating current experiments. *J. Gen. Physiol.* 70:567–590.

Bean, B.P. 1981. Sodium channel inactivation in the crayfish giant axon. Must channels open before inactivating? *Biophys. J.* 35:595–614.

Bean, B.P. 1985. Two kinds of calcium channels in canine atrial cells. Differences in kinetics, selectivity, and pharmacology. *J. Gen. Physiol.* 86:1–30.

Bean, B.P. 1989. Classes of calcium channels in vertebrate cells. *Annu. Rev. Physiol.* 51:367–384.

Bean, B.P., and S.I. McDonough. 1998. Two for T. *Neuron.* 20:825–838.

Bezanilla, F., and C.M. Armstrong. 1977. Inactivation of the sodium channel. I. Sodium current experiments. *J. Gen. Physiol.* 70:549–566.

Berjukow, S., F. Doring, M. Froschmayr, M. Grabner, H. Glossmann, and S. Hering. 1996. Endogenous calcium channels in human embryonic kidney (HEK293) cells. *Br. J. Pharmacol.* 118:748–754.

Bossu, J.-L., and A. Feltz. 1986. Inactivation of the low-threshold transient calcium current in rat sensory neurones: evidence for a dual process. *J. Physiol. (Camb.).* 376:341–357.

Cannon, S.C., and D.P. Corey. 1993. Loss of Na^+ channel inactivation by anemone toxin (ATX II) mimics the myotonic state in hyperkalaemic periodic paralysis. *J. Physiol. (Camb.).* 466:501–520.

Carbone, E., and H.D. Lux. 1984. A low voltage-activated, fully inactivating Ca channel in vertebrate sensory neurones. *Nature.* 310: 501–502.

Carbone, E., and H.D. Lux. 1987. Single low-voltage-activated calcium channels in chick and rat sensory neurones. *J. Physiol. (Camb.).* 386:571–601.

Catterall, W.A. 1996. Molecular properties of sodium and calcium channels. *J. Bioenerg. Biomembr.* 28:219–230.

Chandler, W.K., and H. Meves. 1970. Sodium and potassium currents in squid axons perfused with fluoride solutions. *J. Physiol. (Camb.).* 211:679–705.

Chen, C., and P. Hess. 1990. Mechanism of gating of T-type calcium channels. *J. Gen. Physiol.* 96:603–630.

Cota, G., and C.M. Armstrong. 1989. Sodium channel gating in clonal pituitary cells. The inactivation step is not voltage dependent. *J. Gen. Physiol.* 94:213–232.

Cribbs, L.L., J.-H. Lee, J. Yang, J. Satin, Y. Zhang, A. Daud, J. Barclay, M.P. Williamson, M. Fox, M. Rees, and E. Perez-Reyes. 1998. Cloning and characterization of α1H from human heart, a member of the T-type Ca^{2+} channel gene family. *Circ. Res.* 83:103–109.

Dashti, S.R., J.R. Serrano, L.L. Cribbs, E. Perez-Reyes, and S.W. Jones. 1999. Selectivity of the α1G T-type Ca^{2+} channel. *Biophys. J.* 76:A409. (Abstr.)

DeCoursey, T.E. 1990. State-dependent inactivation of K^+ currents in rat type II alveolar epithelial cells. *J. Gen. Physiol.* 95:617–649.

Fox, A.P., M.C. Nowycky, and R.W. Tsien. 1987. Kinetic and pharmacological properties distinguishing three types of calcium currents in chick sensory neurones. *J. Physiol. (Camb.).* 394:149–172.

Fukushima, Y., and S. Hagiwara. 1985. Currents carried by monovalent cations through calcium channels in mouse neoplastic B lymphocytes. *J. Physiol. (Camb.).* 358:255–284.

Gillespie, J.I., and H. Meves. 1980. The time course of sodium inactivation in squid giant axons. *J. Physiol. (Camb.).* 299:289–307.

Gutnick, M.J., H.D. Lux, D. Swandulla, and H. Zucker. 1989. Voltage-dependent and calcium-dependent inactivation of calcium channel currents in identified snail neurones. *J. Physiol. (Camb.).* 412:197–220.

Herrington, J., and C.J. Lingle. 1992. Kinetic and pharmacological properties of low-voltage-activated Ca^{2+} current in rat clonal (GH_3) pituitary cells. *J. Neurophysiol.* 68:213–232.

Hess, P., J.B. Lansman, and R.W. Tsien. 1986. Calcium channel selectivity for divalent and monovalent cations. Voltage and concentration dependence of single channel current in ventricular heart cells. *J. Gen. Physiol.* 88:293–319.

Hodgkin, A.L., and A.F. Huxley. 1952a. The components of membrane conductance in the giant axon of *Loligo. J. Physiol. (Camb.).* 116:473–496.

Hodgkin, A.L., and A.F. Huxley. 1952b. A quantitative description of membrane current and its application to conduction and excitation in nerve. *J. Physiol. (Camb.).* 117:500–544.

Hoshi, T., W.N. Zagotta, and R.W. Aldrich. 1990. Biophysical and molecular mechanisms of *Shaker* potassium channel inactivation. *Science.* 250:533–538.

Huguenard, J.R. 1996. Low-threshold calcium currents in central nervous system neurons. *Annu. Rev. Physiol.* 58:329–348.

Huguenard, J.R., and D.A. Prince. 1992. A novel T-type current underlies prolonged Ca^{2+}-dependent burst firing in GABAergic neurons of rat thalamic reticular nucleus. *J. Neurosci.* 12:3804–3817.

Huguenard, J.R., and D.A. McCormick. 1992. Simulation of the currents involved in rhythmic oscillations in thalamic relay neurons. *J. Neurophysiol.* 68:1373–1383.

Klemic, K.G., C.-C. Shieh, G.E. Kirsch, and S.W. Jones. 1998. Inactivation of Kv2.1 potassium channels. *Biophys. J.* 74:1779–1789.

Klemic, K.G., G.E. Kirsch, and S.W. Jones. 1999. Two types of slow inactivation of Kv potassium channels. *Biophys. J.* 76:A191. (Abstr.)

Kuo, C.C., and B.P. Bean. 1994. Na^+ channels must deactivate to recover from inactivation. *Neuron.* 12:819–829.

Lambert, R.C., F. McKenna, Y. Maulet, E.M. Talley, D.A. Bayliss, L.L. Cribbs, J.-H. Lee, E. Perez-Reyes, and A. Feltz. 1998. Low-voltage-activated Ca^{2+} currents are generated by members of the Ca_VT subunit family (α1G/H) in rat primary sensory neurons. *J. Neurosci.* 18:8605–8613.

Lee, J.-H., A.N. Daud, L.L. Cribbs, A.E. Lacerda, A. Pereverzev, U. Klockner, T. Schneider, and E. Perez-Reyes. 1999. Cloning and expression of a novel member of the low voltage-activated T-type calcium channel family. *J. Neurosci.* 19:1912–1921.

Lux, H.D., E. Carbone, and H. Zucker. 1990. Na^+ currents through low-voltage-activated Ca^{2+} channels of chick sensory neurones: block by external Ca^{2+} and Mg^{2+}. *J. Physiol. (Camb.).* 430:159–188.

Marom, S., and I.B. Levitan. 1994. State-dependent inactivation of the Kv3 potassium channel. *Biophys. J.* 67:579–589.

Martin, R.L., L.L. Cribbs, E. Perez-Reyes, and D.A. Hanck. 1998. Development of inactivation of the new T-channel, α1G, expressed in mammalian cells. *Soc. Neurosci. Abstr.* 24:1823. (Abstr.)

Meir, A., and A.C. Dolphin. 1998. Known calcium channel α_1 subunits can form low threshold small conductance channels with similarities to native T-type channels. *Neuron.* 20:341–351.

Mitrovic, N., A.L. George, Jr., and R. Horn. 1998. Independent versus coupled inactivation in sodium channels. Role of the domain 2 S4 segment. *J. Gen. Physiol.* 111:451–462.

Nakashima, Y.M., S.M. Todorovic, A. Pereverzev, J. Hescheler, T. Schneider, and C.J. Lingle. 1998. Properties of Ba^{2+} currents arising from human α1E and α1Eβ3 constructs expressed in HEK293 cells: physiology, pharmacology, and comparison to native T-type Ba^{2+} currents. *Neuropharmacology.* 37:957–972.

Narahashi, T., A. Tsunoo, and M. Yoshii. 1987. Characterization of two types of calcium channels in mouse neuroblastoma cells. *J. Physiol. (Camb.).* 383:231–249.

Neher, E., and H.D. Lux. 1971. Properties of somatic membrane patches of snail neurones under voltage clamp. *Pflügers Arch.* 322: 35–38.

Nilius, B., P. Hess, J.B. Lansman, and R.W. Tsien. 1985. A novel type of cardiac calcium channel with different calcium sensitivity. *Nature.* 316:443–446.

Nowycky, M.C., A.P. Fox, and R.W. Tsien. 1985. Three types of neuronal calcium channel with different calcium agonist sensitivity. *Nature.* 316:440–443.

Patil, P.G., D.L. Brody, and D.T. Yue. 1998. Preferential closed-state inactivation of neuronal calcium channels. *Neuron.* 20:1027–1038.

Perez-Reyes, E., L.L. Cribbs, A. Daud, A.E. Lacerda, J. Barclay, M.P. Williamson, M. Fox, M. Rees, and J.-H. Lee. 1998. Molecular characterization of a neuronal low-voltage-activated T-type calcium channel. *Nature.* 391:896–900.

Raman, I.M., and B.P. Bean. 1997. Resurgent sodium current and action potential formation in dissociated cerebellar Purkinje neurons. *J. Neurosci.* 17:4517–4526.

Randall, A.D., and R.W. Tsien. 1997. Contrasting biophysical and pharmacological properties of T-type and R-type calcium channels. *Neuropharmacology.* 36:879–893.

Shuba, Y.M., V.I. Teslenko, A.N. Savchenko, and N.H. Pogorelaya. 1991. The effect of permeant ions on single calcium channel activation in mouse neuroblastoma cells: ion-channel interaction. *J. Physiol. (Camb.).* 443:25–44.

Soong, T.W., A. Stea, C.D. Hodson, S.J. Dubel, S.R. Vincent, and T.P. Snutch. 1993. Structure and functional expression of a member of the low voltage-activated calcium channel family. *Science.* 260:1133–1136.

Todorovic, S.M., and C.J. Lingle. 1998. Pharmacological properties of T-type Ca^{2+} current in adult rat sensory neurons: effects of anticonvulsant and anesthetic agents. *J. Neurophysiol.* 79:240–252.

Vandenberg, C.A., and F. Bezanilla. 1991. Single-channel, macroscopic, and gating currents from sodium channels in the squid giant axon. *Biophys. J.* 60:1499–1510.

Wang, X.-J., J. Rinzel, and M.A. Rogawski. 1991. A model of the T-type calcium current and the low-threshold spike in thalamic neurons. *J. Neurophysiol.* 66:839–850.

Williams, S.R., T.I. Toth, J.P. Turner, S.W. Hughes, and V. Crunelli. 1997. The 'window' component of the low threshold Ca^{2+} current produces input signal amplification and bistability in cat and rat thalamocortical neurones. *J. Physiol. (Camb.).* 505:689–705.

Zhu, G., Y. Zhang, H. Xu, and C. Jiang. 1998. Identification of endogenous outward currents in the human embryonic kidney (HEK 293) cell line. *J. Neurosci. Methods.* 81:73–83.